CONVECTIVE BOILING HEAT TRANSFER OF THE n-PENTANE INSIDE AN ANNULAR MICROCHANNEL

Evandro Rodrigo Dário, Gil Goss Júnior, Júlio César Passos

Departamento de Engenharia Mecânica, LEPTEN/Boiling, Universidade Federal de Santa Catarina
88040-900 Florianópolis, SC, Brazil. E-mails: rdario@lepten.ufsc.br; jpassos@emc.ufsc.br

ABSTRACT

An experimental study is here presented on heat transfer in the convective boiling of n-Penane, C_5H_{12}, in an annular microchannel, for input pressures and temperatures in the test section of 150 and 200 kPa, and 27 and 40°C, respectively. Mass velocity of up to 338 kg/m^{2}s for heat flux q" ≤ 60.0 kW/m^2 was employed. The test section is composed of two tubes, one inner copper tube where the heating is performed, and the other outer acrylic tube, mounted concentrically, with a gap between them of 0.25 mm, thus forming an annular minichannel with a hydraulic diameter of 0.5 mm. The effects of mass velocity, input pressure and temperature, and heat flux on the heat transfer coefficients for boiling were investigated. Experimental data for the heat transfer coefficients were compared with the correlations of Liu and Winterton (1991), Steiner and Taborek (1992) and Warrier et al. (2002). A summary of the visualization of the flow related to the process of convective boiling in the microchannel are also presented.

INTRODUCTION

The rapid development of industrial applications for micro-devices, micro-systems, advanced material design, and micro-manufacturing is creating a strong demand for a better understanding of micro-scale transport phenomena and is causing a notable shift in thermal science and heat transfer research from the macro- to micro-scale, as reported by Peng and Wang [1].

Boiling in microchannels and microstructures is an important topic in this area and has a particular significance in the development of new technologies and devices for control of energy transfer and other advanced applications requiring very compact and extremely large heat flux heat exchangers. The investigations of microscale transport processes conducted in the past decade have shown that microscale transport processes have distinct thermal fluid flow, heat transfer, and other thermal transport phenomena as compared to conventional situations, as reported by Wen et. al. [2]. Experimental data in the literature also demonstrate that the boiling characteristics in microchannels can be different from those in macrochannels, although there isn't sufficient research available on the subject.

Thus, only part of the knowledge available on macroscale heat transfer can be transferred to the microscale, but it is not clear exactly what is still valid and what is not. In other words, there still not a recognized transition threshold criterion from macroscale to microscale clearly defined for two-phase processes. Several classifications for this transition, based on the hydraulic diameter, D_h, for non-circular channels have been proposed.

Kandlikar [3] recommends the following classification and size ranges based on the D_h: microchannels (50–600 μm), minichannels (600 μm to 3 mm) and conventional channels (D_h > 3 mm). Such transition criteria are arbitrary and do not reflect the influence of the channel size on the physical mechanisms.

A better macro-to-micro transition criterion might be related to the bubble departure diameter. When the channel diameter is equal to or smaller than the capillary length, any additional increase in the bubble the coalescence of two or more bubbles will cause its deformation. In this case the confinement caused by the small space inside the channel will stretch the bubbles.

Kew and Cornwell [4] recommend using the confinement number, N_{CO}, as a criterion to differentiate between macroscale and microscale two-phase flow and heat transfer, defined according to Eq. (1).

$$N_{CO} = \left[\frac{\sigma}{g\left(\rho_g - \rho_g\right) D_h^2} \right]^{1/2} \tag{1}$$

where σ, g, ρ_f and ρ_g represent the surface tension, the acceleration due to gravity, the liquid and the vapor density, respectively. They reported that the heat transfer and flow characteristics differed significantly to those observed in macrochannels for N_{Co} > 0.5. Hence, a second criterion for the transition between macro- and micro-scale, is adopted in this study:

Microchannel: $N_{CO} > 0.5$
Macrochannel: $N_{CO} < 0.5$

For n-Pentane at atmospheric pressure, T_{sat} = 36°C, the capillary length for this criterion is 3.2 mm and this becomes smaller as the saturation pressure increases.

Various investigators, such as Bowers and Mudawar [5], have recently demonstrated that the flow passage geometry has a significant impact on boiling, bubble generation and bubble growth in microchannels. The concept of 'evaporating space', as was reported by Peng and Wang [6], suggests that there is a minimum amount of space necessary to generate a vapor bubble in a confined microchannel. In fact, bubble size has long been considered as a critical parameter in understanding the nucleate boiling characteristics and the dynamic bubble processes.

The objective of this study is to investigate the heat transfer in a two-phase flow of n-Pentane in an annular microchannel, varying the mass velocity, heat flux, pressure, and subcooling at the entrance of the test section. The results for the boiling heat transfer coefficient, h_{tp}, will be compared with two different correlations developed for flow boiling in micro and macro (or conventional) channels.

EXPERIMENT

Experimental Apparatus

Figure 1 shows a schema of the experimental setup, for which the design and construction of convective boiling circuit and the test section were carried out at LEPTEN/Boiling – "Laboratory of Heat Transfer with Phase Change and Two-Phase Flow". The test loop consists of a magnetic gear pump; a pre-heater reservoir; a pre-heater, consisting of three tubes in line with a total length of 1.32 m; a mass flow meter, a condenser and a reservoir.

The working fluid is cooled in the condenser, located after the test section. The cooling system uses water as the cold fluid. The water cooling system is a LAUDA RK20 KP cryostat.

Figure 2 shows a sketch of the test section, in an exploded view, which comprises a copper tube with 29.9 mm diameter and 4.6 mm thickness. Inside this tube, seven type-E thermocouples of 0.3 mm diameter were inserted, located at the entrance, center and exit of the test section. The copper tube is heated by a cartridge-type electrical resistance inserted in its interior, which supplies the flow of heat imposed by the experiment. The copper tube is surrounded by a transparent acrylic tube, forming a mini channel which allows the visualization of the two-phase flow through it. To minimize the thermal losses to the atmosphere, the whole test section was insulated with glass wool.

The test section contained plena both upstream and downstream of the micro-channels to ensure even flow distribution, as can be seen in Figure 2.

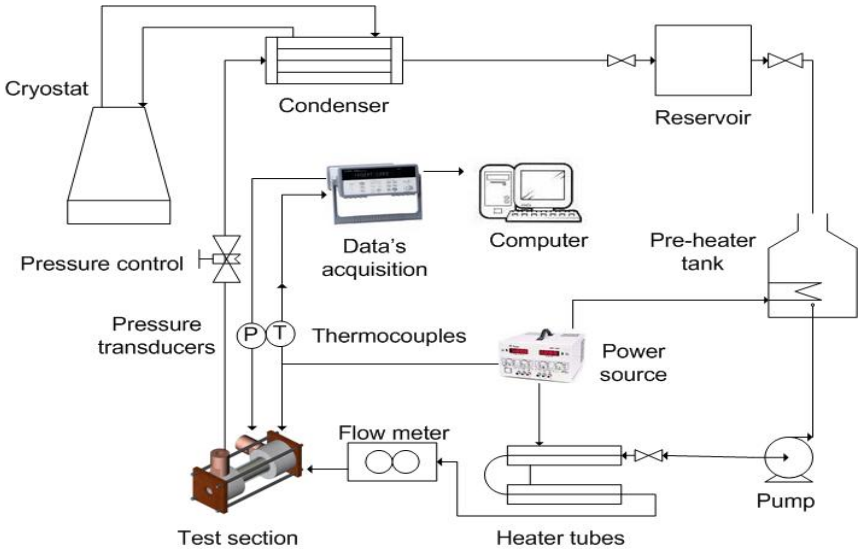

Figure 1 - Sketch of the experimental setup

In the reservoir pre-heater, located before the gear pump, the working fluid is heated to a temperature close to the saturation temperature in order to eliminate gases which could be dissolved in the fluid. This heating is accomplished by two cartridge-type resistors, inserted inside the reservoir. A relief valve, located at the top of the tank allows the elimination of gases to the outside. It also has a mixer to homogenize the temperature of the fluid in its interior.

By means of the gear pump, the mass flow rate is controlled during the two-phase flow tests in the range that could be tested, i.e., 40 to 400 kg/m^2 s.

The pre-heater tubes (three parallel steel tubes) are used to maintain the working fluid at the desired temperature at the entrance of the test section. The heat flux is accomplished through the Joule effect via a NiCr tape wound around the pre-heater tubes.

The fluid temperature in the pre-heater tubes is controlled through type-E thermocouples inserted at their inlet and outlet of the tubes. The power required for the heating is controlled automatically using the Labview software.

The mass flow rate is measured using a Coriolis flow meter with an uncertainty of ± 0.2 % in the reading. A valve, placed after the test section, controls the pressure during the experiment. Pressure is measured with two pressure transducers located at the entrance and exit of the test section.

Two absolute pressures and two type-E thermocouple transducers are installed directly before the two plena to measure the inlet and outlet pressure and temperature.

The DC power supply, is connected to the skin heater and controlled by a PC using Labview software. The acquisition and previous data treatment are carried out with an HP34970A system.

The temperature uncertainty was ± 0.6ºC.

Experimental Procedure

Before the test begins, the reservoir is evacuated, passing all of the n-Pentane to the reservoir pre-heater. Raising the temperature of the fluid to a temperature close to its saturation temperature forces the elimination of any dissolved gases, discharging them to the atmosphere. The flow loop components are then adjusted to give the desired module inlet temperature, T_{in}, mass velocity, G, and inlet pressure, P_{in}, in test section.

When the desired conditions are reached, the test begins applying small increases in the heat flux at the test section. The conditions at the beginning of the test were maintained throughout the test.

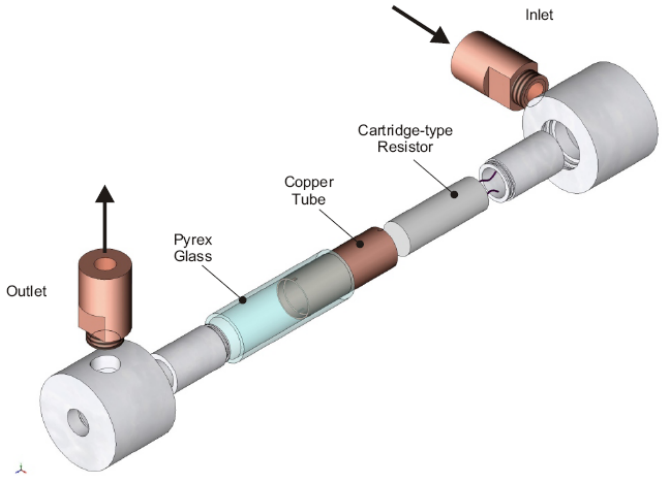

Figure 2 – Exploded view of test section

For all test conditions, the working fluid was subcooled ($T_{in} < T_{sat}$) at the entrance of the test section.

The microchannels can be divided into two regions: an upstream sub-cooled inlet region and a downstream saturated region; the location of zero thermodynamic equilibrium ($x_e = 0$) serves as a dividing point between the two regions. The length of the two regions can be evaluated using Eq. (2):

$$L_{sub} = \frac{\dot{m} c_{pl} \left(T_{sat,0} - T_{in} \right)}{q^{"}_{ch} P_{wet}} \tag{2}$$

where $\dot{m}$ represents the mass flow, T_{sat} the saturation temperature of n-Pentane at the location where x_e is zero, T_{in} the entrance temperature of the test section, P_{wet} the wetted perimeter, $q^{"}_{ch}$ is the heat flux imposed on the external surface of the copper tube, c_{pf} the liquid specific heat of n-Pentane at T_{sat}, and L_{sub} the length of the sub-cooled area. Thereafter, L_{sat} is defined by Eq. (3).

$$L_{sat} = L - L_{sub} \tag{3}$$

where L and L_{sat} represent the length of the microchannel and the length of the two-phase flow regions, respectively.

The determination of the local flow boiling heat transfer coefficient requires knowledge of the local fluid temperature, microchannel wall temperature and heat flux. Since sub-cooled boiling may occur upstream of the point of zero thermodynamic equilibrium, the heat transfer coefficient can be accurately evaluated only at stream-wise locations which are in the saturate region ($x_e \geq 0$), and where the heat sink temperatures are measured by thermocouples. For the present test conditions, the two upstream thermocouples were mostly within the sub-cooled region. Therefore, only the saturated heat transfer coefficient results that were obtained at the center and outlet locations are of interest.

The saturation temperature, T_{sat}, is based on the local pressure. The pressure at the location of $x_e = 0$ can be considered very close to that measured at the channel inlet, P_{in}. Taking into account the value of the pressure measured at the channel outlet, P_{out}, a linear interpolation was carried out to determine the pressure at the cross section where the wall thermocouples are installed and then the saturation temperature T_{sat} was determined. This procedure for estimation of the saturation temperature is based on the relatively small pressure drop (< 20 kPa) in the present study. The value of the heat transfer coefficient, h_{tp}, can be determined from the following equation:

$$h_{tp} = \frac{q^{"}_{ch}}{(T_w - T_{sat})} \tag{4}$$

where T_w represents the wall temperature and T_w-T_{sat} represents the local wall superheat.

In the next section, the experimental results for n-Pentane confined nucleate boiling in the mini channel will be presented and discussed for heat fluxes of 7.5 to 60 kW/m^2 and for mass flow rates of 85 to 338 kg/m^2 s.

In the next section, the experimental results for n-Pentane confined nucleate boiling in the mini channel will be presented and discussed for heat fluxes of 7.5 to 60 kW/m^2 and for mass flow rates of 85 to 338 kg/m^2 s.

The experimental uncertainties in the boiling heat transfer coefficient decreased with an increase in the heat flux. For 7.5 $<q^{"}_{ch}<$20 kW/m^2 it was 9.0%, for 22.5 $< q^{"}_{ch} <$40 kW/m^2 it was 6.9% and for 42.5 $< q^{"}_{ch} <$60 kW/m^2 was 6.2% of the h_{tp}.

Tests in single-phase were first performed to determine the heat loss to the environment and to validate the experimental apparatus and procedure. The rate of heat transfer to the fluid can be measured by applying a macroscopic energy balance: $mc_{pl}(T_{out}-T_{in})$, and the measured power input is the product of the voltage and the current. The difference between the calculated rate of heat transfer to the fluid and the measured power input was less than 3%. (15)

The saturation temperature, $T_{sat,z}$, at any distance z from the inlet, is a function of the local, $P_{sat,z}$, which can be determined by the difference between the measured output pressure, $P_{sat,out}$, and the pressure drop of the two-phase flow region $\Delta P_{two\text{-}phase,z,out}$, as is shown in the following equations

$$P_{sat,z} = P_{sat,out} - \Delta P_{two\text{-}phase,z,out} \tag{5}$$

$$T_{sat,z} = f(P_{sat,z}) \tag{6}$$

(16)

The last parameter was determined using the two-phase flow basic models, spareted flow or homogeneous model, Collier [16].

A visualization of the flow boiling was provided by taking photographs with a Canon camera (EOS Digital Rebel) a 6.3 mega pixel lens (Ef 100mm f/2.8 Macro USM).

RESULTS AND DISCUSSION

Partial boiling curves and heat transfer coefficient

Figure 3 shows the partial boiling curves obtained in this study, where the flow is subcooled to 7.9°C at the entrance of the micro-channel. For low heat fluxes, i.e. lower than the onset of nucleate boiling, (ONB), temperature, the heat transfer mode is single-phase flow forced convection and the ONB occurs for thermal superheats and the heat flux increases with the increase in mass velocity G. By increasing the heat flux gradually during the tests, the temperature of the heated wall of the mini-channel also increases slowly. When the wall superheat T_w-T_{sat} reaches a critical level, a small increase in the heat flux is sufficient to

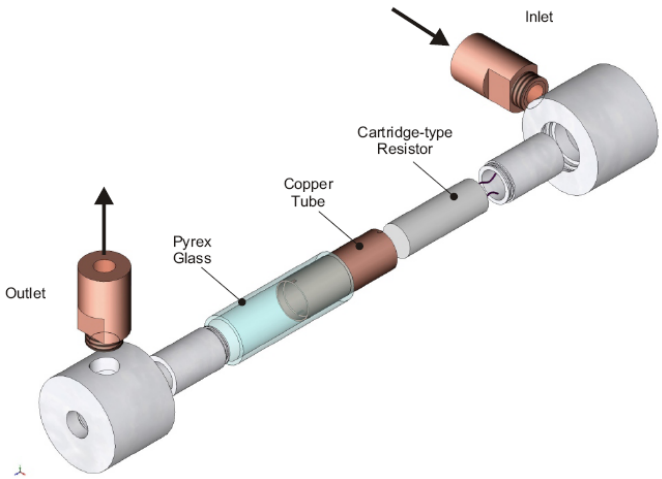

Figure 2 – Exploded view of test section

For all test conditions, the working fluid was subcooled ($T_{in} < T_{sat}$) at the entrance of the test section.

The microchannels can be divided into two regions: an upstream sub-cooled inlet region and a downstream saturated region; the location of zero thermodynamic equilibrium ($x_e = 0$) serves as a dividing point between the two regions. The length of the two regions can be evaluated using Eq. (2):

$$L_{sub} = \frac{\dot{m} c_{pl} \left(T_{sat,0} - T_{in} \right)}{q''_{ch} P_{wet}} \tag{2}$$

where $\dot{m}$ represents the mass flow, T_{sat} the saturation temperature of n-Pentane at the location where x_e is zero, T_{in} the entrance temperature of the test section, P_{wet} the wetted perimeter, q''_{ch} is the heat flux imposed on the external surface of the copper tube, c_{pf} the liquid specific heat of n-Pentane at T_{sat}, and L_{sub} the length of the sub-cooled area. Thereafter, L_{sat} is defined by Eq. (3).

$$L_{sat} = L - L_{sub} \tag{3}$$

where L and L_{sat} represent the length of the microchannel and the length of the two-phase flow regions, respectively.

The determination of the local flow boiling heat transfer coefficient requires knowledge of the local fluid temperature, microchannel wall temperature and heat flux. Since sub-cooled boiling may occur upstream of the point of zero thermodynamic equilibrium, the heat transfer coefficient can be accurately evaluated only at stream-wise locations which are in the saturate region ($x_e \geq 0$), and where the heat sink temperatures are measured by thermocouples. For the present test conditions, the two upstream thermocouples were mostly within the sub-cooled region. Therefore, only the saturated heat transfer coefficient results that were obtained at the center and outlet locations are of interest.

The saturation temperature, T_{sat}, is based on the local pressure. The pressure at the location of $x_e = 0$ can be considered very close to that measured at the channel inlet, P_{in}. Taking into account the value of the pressure measured at the channel outlet, P_{out}, a linear interpolation was carried out to determine the pressure at the cross section where the wall thermocouples are installed and then the saturation temperature T_{sat} was determined. This procedure for estimation of the saturation temperature is based on the relatively small pressure drop (< 20 kPa) in the present study. The value of the heat transfer coefficient, h_{tp}, can be determined from the following equation:

$$h_{tp} = \frac{q''_{ch}}{(T_w - T_{sat})} \tag{4}$$

where T_w represents the wall temperature and T_w-T_{sat} represents the local wall superheat.

In the next section, the experimental results for n-Pentane confined nucleate boiling in the mini channel will be presented and discussed for heat fluxes of 7.5 to 60 kW/m^2 and for mass flow rates of 85 to 338 kg/m^2 s.

The experimental uncertainties in the boiling heat transfer coefficient decreased with an increase in the heat flux. For 7.5 $< q''_{ch} <$20 kW/m^2 it was 9.0%, for 22.5 $< q''_{ch} <$40 kW/m^2 it was 6.9% and for 42.5 $< q''_{ch} <$60 kW/m^2 was 6.2% of the h_{tp}.

Tests in single-phase were first performed to determine the heat loss to the environment and to validate the experimental apparatus and procedure. The rate of heat transfer to the fluid can be measured by applying a macroscopic energy balance: $mc_{pl}(T_{out}$-$T_{in})$, and the measured power input is the product of the voltage and the current. The difference between the calculated rate of heat transfer to the fluid and the measured power input was less than 3%.

The saturation temperature, $T_{sat,z}$, at any distance z from the inlet, is a function of the local, $P_{sat,z}$, which can be determined by the difference between the measured output pressure, $P_{sat,out}$, and the pressure drop of the two-phase flow region $\Delta P_{\text{two-phase,z,out}}$, as is shown in the following equations.

$$P_{sat,z} = P_{sat,out} - \Delta P_{\text{two-phase,z,out}} \tag{5}$$

$$T_{sat,z} = f(P_{sat,z}) \tag{6}$$

The last parameter was determined using the two-phase flow basic models, spareted flow or homogeneous model, Collier [16].

A visualization of the flow boiling was provided by taking photographs with a Canon camera (EOS Digital Rebel) a 6.3 mega pixel lens (Ef 100mm f/2.8 Macro USM).

RESULTS AND DISCUSSION

Partial boiling curves and heat transfer coefficient

Figure 3 shows the partial boiling curves obtained in this study, where the flow is subcooled to 7.9°C at the entrance of the micro-channel. For low heat fluxes, i.e. lower than the onset of nucleate boiling, (ONB), temperature, the heat transfer mode is single-phase flow forced convection and the ONB occurs for thermal superheats and the heat flux increases with the increase in mass velocity G. By increasing the heat flux gradually during the tests, the temperature of the heated wall of the mini-channel also increases slowly. When the wall superheat T_w-T_{sat} reaches a critical level, a small increase in the heat flux is sufficient to cause the sudden appearance of small vapor bubbles followed by a rapid drop in the wall temperature.

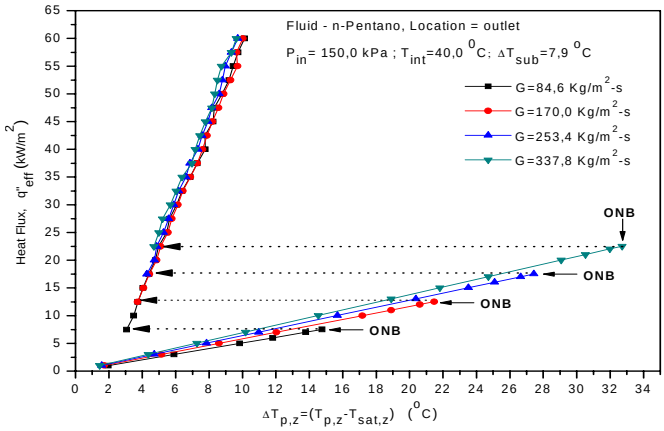

Figure 3- Partial boiling curves

The effect of the mass velocity G on the ONB wall superheat can be summarized for cases where G is 84.6 and 337.8 kg/m^2 and the wall superheat, as is shown in Fig. 3, is 12 and 29 ^{o}C, respectively.

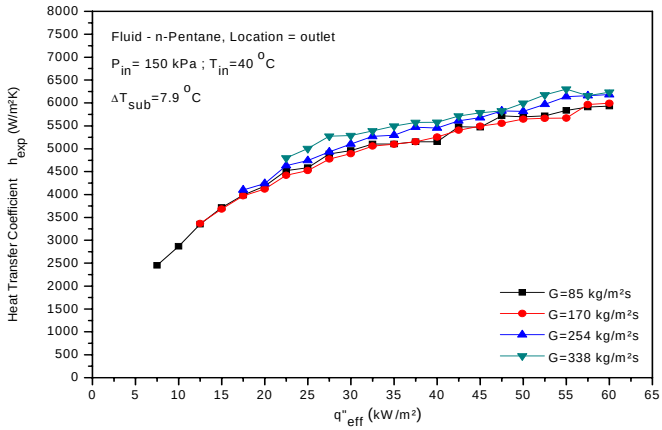

Figure 4 – Effect of mass velocity on heat transfer coefficients

As expected, for heat fluxes higher than those corresponding to the ONB condition the slope of the curves becomes much more pronounced in the two-phase flow region, compared with the region of single-phase forced convection, indicating a higher heat transfer coefficient.

Figure 4 shows the effect of the mass velocity on the heat transfer coefficients for 84.6 kg/m^{2}s, 170 kg/m^{2}s, 253.4 and 337.8 kg/m^{2}s, where the pressure and temperature at the entrance of the test section was 200 kPa and 40°C, respectively. The increase in the mass velocity causes a small increase of the heat transfer coefficient. For a particular mass velocity, the heat transfer coefficient increases with the increase in the heat flux, as occurs for the nucleate boiling regime. The trend of results is that the convective boiling regime was reach only for the two higher mass velocity values. The trend of results obtained in this study is similar to that of the results published by several authors, for instance, Zhao et al [15] and Pettersen [14].

Figure 5 shows the experimental points for n-Pentane, for a mass velocity constant of 84.6 kg/m^{2}s and pressure at the entrance of the test section of 200 kPa, for two input temperatures of 27 and 40^{o}C, resulting in sub-coolings of 17.5 and 30.5^{o}C.

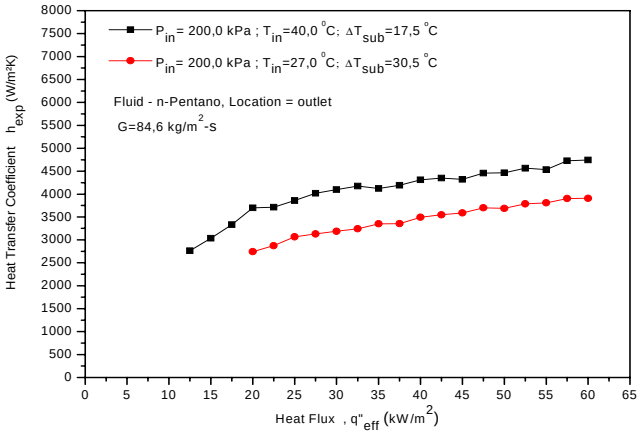

Figure 5 – Coefficients of heat transfer as function of the inlet subcooled of the flow

The decrease in the inlet of sub-cooling increases the heat transfer coefficient. It is important to note that for a given mass velocity, the lower the degree of sub-cooling at the entrance test section, the greater the value of vapor quality at exit of the microchannel For example, for a degree of sub-cooling of 7.9 °C, the vapor quality attains more than 60% at the output section of the test.

Empirical correlations

The experimental results for the local heat transfer coefficient were compared with those calculated by two empirical correlations, developed for flow boiling in microchannels and also for conventional channels.

Bai et al. [7] proposed that when the cross section of the channel is annular, of which only the inner surface is heated, the equivalent diameter is defined by the following equation:

$$D_{e,H} = \frac{4A_c}{P_H} = \frac{4\frac{\pi}{4}(d_o^2 - d_i^2)}{\pi d_i^2} = \frac{(d_o^2 - d_i^2)}{d_i} \qquad (7)$$

where d_o, d_i, A_c and P_H represent the outer and inner diameters, the cross sectional area and the heated perimeter of the annulus channel, respectively. Unlike the hydraulic diameter, normally recommended for channels with cross sections distinct from circular ones, the equivalent diameter defined by Eq. (7) takes into account the non uniformity of the heating along the channel, because the outer surface is insulated.

The correlations tested in the present study are summarized in the Appendix of this manuscript.

Figures 6 to 8 show a comparison of the experimental results for the heat transfer coefficient with those calculated by the correlations of Liu and Winterton [10], as shown in the Appendix, Eq. (A1), Steiner and Taborek [11], as shown in the Appendix, Eq. (A2), and Warrier et al. [12], shown in the Eq. (A3). Among these three correlations, the first two were obtained for conventional channels. Whereas that of Warrier et al. [12] was obtained for microchannels.

The ability of each correlation to predict the experimentals results is characterized by the mean absolute error (MAE), defined as:

$$MAE = \frac{100}{N}\sum_{n=1}^{N}\left|\frac{h_{tp,exp} - h_{tp,cor}}{h_{tp,exp}}\right| \quad (8)$$

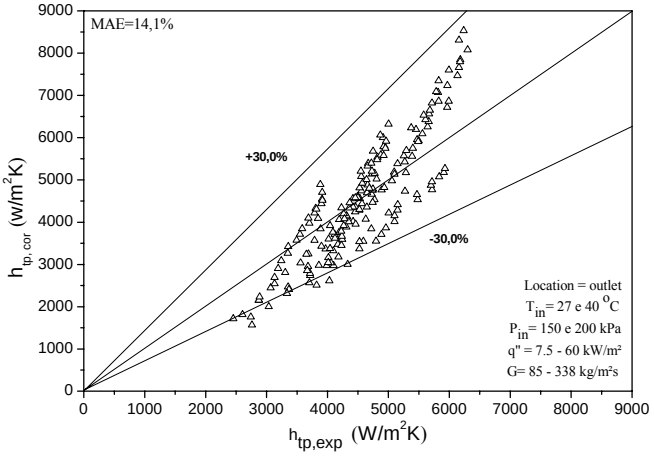

Figure 6 – Experimental data versus the correlation of Liu and Winterton (1991) [10].

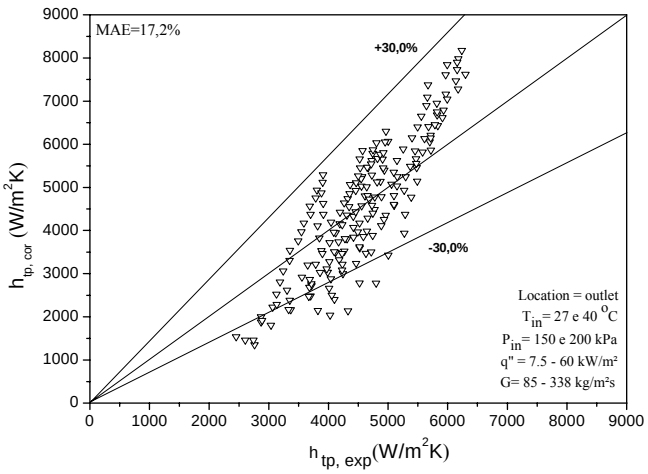

Figure 7 – Experimental data versus the correlation of Steiner and Taborek (1992) [11].

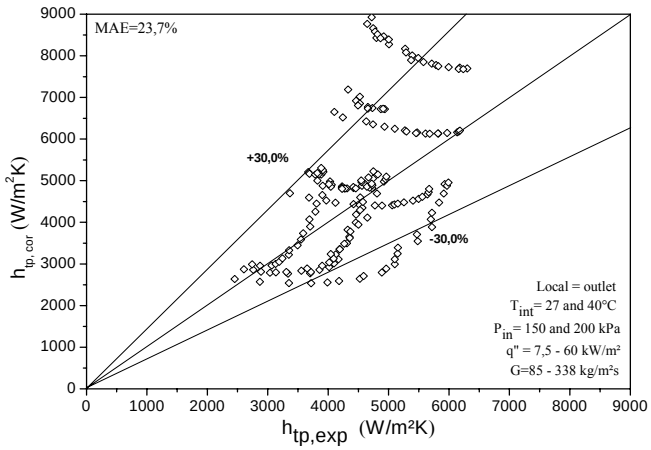

Figure 8 – Experimental data versus the correlation of Warrier et al. (1992) [12].

The best agreement between the experimental data and the correlations tested was obtained for that Liu and Winterton [10], with an MAE of 14.1%, whereas this one of Steiner and Taborek [11] gave an MAE of 17.2%. Compared with the correlation of Warrier et al. [12], the MAE is 23.7%, noting that this was the only tested correlation obtained from microchannel data on convective boiling. Two other correlations were tested: that of Kandlikar [9], with an MAE of 52% and obtained for conventional channels, and that of Lazarek and Black [8], with an MAE of 55% (obtained for microchannels).

Flow visualization

In this section, four ensembles of photographs taken during the boiling flow inside the annulus microchannel are presented. In Figures 9 to 12, the flow direction is from right to left.

Figure 9 shows the influence of the heat flux during the boiling flow for a mass velocity of 148.0 kg/m^{2}s. For all heat fluxes there is a trend for the vapor phase to stratify in the

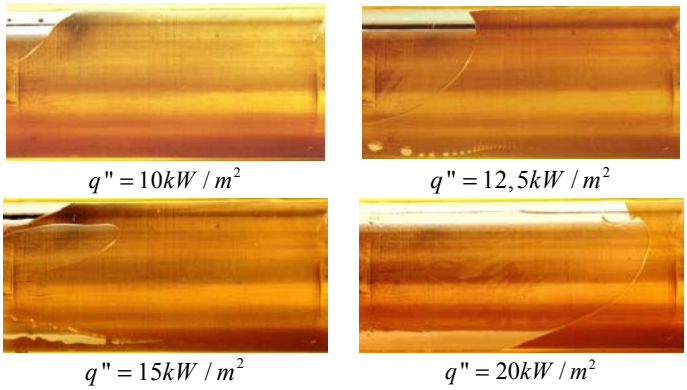

Figure 9 – G = 148.0 kg/m^{2}s

upper part of the test section. For a heat flux of 12.5 kW/m^2 there is the appearance of a nucleation site the bottom center of the microchannel, and in the wake of the flow. The increase in the heat flux is followed by faster growth of the bubbles and (almost) only a single long bubble is observed in the final half of the microchannel, near the exit of the microchannel.

In Figure 10, for a mass velocity of 190 k/m^{2}s, the number of nucleation sites present when the heat flux is 20 kW/m^2 increases more rapidly with the increase in heat flux and large vapor bubbles are created by coalescence.

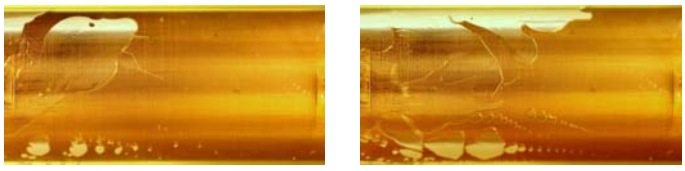

Figure 10 – G = 190.0 kg/m^{2}s

Figures 11 and 12 show photographs taken for higher mass velocities. On increasing heat flux the two-phase flow appears to be much more unstable, not presenting a clear definition of the interface between the liquid and vapor as was noted for the lower mass velocities, in the case of Figure 9.

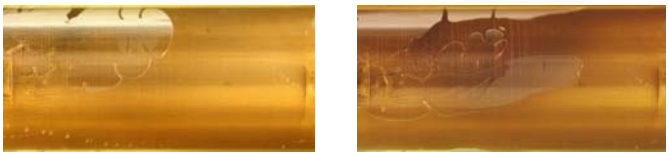

$q" = 17,5kW/m^2$ $q" = 20kW/m^2$

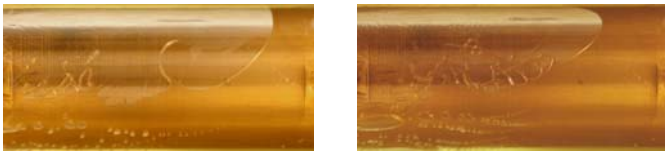

$q" = 25kW/m^2$ $q" = 30kW/m^2$

Figure 11 – G = 232.0 kg/m^{2}s

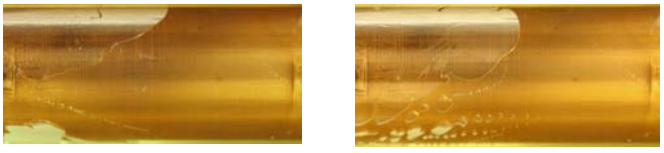

$q" = 20kW/m^2$ $q" = 25kW/m^2$

$q" = 30kW/m^2$

Figure 12 – G = 274.0 kg/m2s

Figures 9 to 12 show the progression of the vapor-liquid interface moving upstream of the microchannel and it is characterized by a, trend toward the, formation of an elongated and flattened bubble. There is a transient existence of large vapor bubbles that can grow in the longitudinal direction as well as in the circumferential direction, evebtually forming, in most cases, large pockets of vapour that can cover the entire circumference of the copper tube.

CONCLUSIONS

This manuscript summarizes the results obtained during an experimental investigation on the boiling flow of n-Pentane inside an annulus microchannel with d_h = 0.5 mm. The test conditions were: 85 < G < 338 kg/m^{2}s, 0 < q" < 60 kW/m^2, inlet temperatures of 27 and 40 ºC and inlet pressure of 150 and 200 kPa.

Key findings from the study are as follows:

(i) The wall superheat for the ONB increases with the increase in mass velocity (G).
(ii) A decrease of the inlet sub-cooling increases the heat transfer coefficient.
(iii) The variation of mass velocity showed a little effect on the heat transfer coefficient, indicating that the heat transfer mechanisms is characterized by the nucleate boiling and only for higher mass velocity, G > 170 kg/m^{2}s, can the convective effect be noted.
(iv) The use of the equivalent heated diameter was partially verified as a good approach to compare the experimental heat transfer coefficients for an annulus microchannel with values calculated by the empirical correlations.
(v) Relatively good agreements were obtained by comparing the experimental heat transfer coefficients with the values calculated by the correlations of Liu and Winterton [10], with an MAE of 14.1%, Steiner and Taborek [11], with an MAE of 17.2%, and Warrier et al. [12], with an MAE of 23.7%.
(vi) With the increase in mass velocity, particularly for cases where heat flow is higher, the flow appears to be much more unstable, not presenting the clear definition of the interface between the liquid and vapor noted for lower mass velocities.

ACKNOWLEDGEMENTS

The authors are grateful for the support of CAPES and CNPq in the performance of this study. The experimental setup was financed by a project approved by the UNIVERSAL project of CNPq.

NOMENCLATURE

Symbol	Quantity	SI
g	acceleration due to gravity	m/s^2
h	heat transfer coefficient	W/m^{2}K
h_{lv}	latent heat of vaporization	kJ/kg
L	length	m
q	heat flux	kW/m^2
T	temperature	K
N	number	-
D,d	diameter	m
$\dot{m}$	mass flux	kg/s
M_w	molar mass	kg/kmol
G	mass velocity	kg/m^{2}s
P	perimeter	m
c_p	specific heat	J/kgK
MAE	mean absolute error	-

Greek symbols

ΔT	wall superheating
ρ	density
σ	surface tension

Subscripts

l	liquid
lv	liquid-vapor
sat	saturation
v	vapor
w	wall
CO	confinement
sub	sub-cooled
i	inlet
o	outlet

h	hydraulic
ch	channel
tp	two-phase
cor	correlation
exp	experimental
wet	wetted
H	heated
E	equivalent
eff	effective

REFERENCES

1. X F. Peng and B.X. Wang, Forced convection and boiling characteristics in microchannels, *Proceedings of the 11th International Heat Transfer*, vol. 1, Kyonji, Korea, 23–28 August, pp. 371–390, 1998.
2. D.S. Wen, Youyou Yan and D.B.R. Kenning, Saturated flow boiling of water in a narrow channel: time-averaged heat transfer coefficients and correlations, Applied Thermal Engineering, vol. 24, Issues 8-9, pp. 1207-1223, 2004.
3. S.G. Kandlikar, Fundamental issues related to flow boiling in minichannels and microchannels, Exp. Therm. Fluid Sci., vol. 26, pp. 389–407, 2002.
4. P. Kew, K. Cornwell, Correlations for prediction of boiling heat transfer in small diameter channels. Applied Thermal Engineering, vol. 17, Issues 8–10, pp. 705–715, 1997.
5. M.B. Bowers and I. Mudawar, High flux boiling in low flow rate, low pressure drop mini-channel and microchannel heat sinks, International Journal of Heat and Mass Transfer, vol. 37, pp. 321-332, 1994.
6. X.F. Peng and B.X. Wang, Forced-low convection and flow boiling heat transfer for liquid flowing through microchannels, International Journal of Heat and Mass Transfer, vol. 36, pp. 3421-3427, 1993.
7. B.F. Bai, R. Huang, L.J. Guo and Z.J. Xiao, Physical model of critical heat flux with annular flow in annulus tubes, J. Eng. Thermophys, vol. 24, pp. 251–254, 2003.
8. G.M. Lazarek and S.H. Black, Evaporative heat transfer, pressure drop and critical heat flux in a small vertical tube with R-113, International Journal of Heat and Mass Transfer, vol. 25, pp. 945–960, 1982.
9. S.G. Kandlikar, A general correlation for saturated two-phase vertical tubes, Journal of Heat Transfer, vol. 112, pp. 219–228, 1990.
10. Z. Liu and R.H.S. Winterton, A general correlation for saturated and subcooled flow boiling in tube and annuli, International Journal of Heat and Mass Transfer, vol. 34, pp. 2759–2766, 1991.
11. D. Steiner and J. Taborek, Flow boiling heat transfer in vertical tubes correlated by an asymptotic model, Heat Transfer Eng. , vol. 13, pp. 43–69, 1992.
12. G.R. Warrier, V.K. Dhir and L.A. Momoda, Heat transfer and pressure drop in narrow rectangular channel, Exp. Therm. Fluid Sci., vol. 26, pp. 53–64, 2002.
13. J. Pettersen, Flow vaporization of CO2 in microchannel tubes. Exp. Thermal Fluid Science, 28, pp. 111-121, 2004.
14. R. Yun, Y. Kim and M. Kim, Convective Boiling Heat Transfer Characteristics of CO2 in Microchannels. International Journal of Heat and Mass Transfer, 48, pp. 235-242, 2005.
15. Y. Zhao, M. Molki, M. Ohadi and S.V. Dessiatoun, Flow boiling of CO2 in microchannels, ASHRAE Trans, 106, pp. 437-445, 2000.
16. Collier, J., & Thome, J. Convective boiling and condensation (3 ed.). Oxford: Clarendon Press, (1996).

Appendix

Flow Boiling heat transfer correlations

Liu and Winterton 1991, [10]	$h_{tp} = \left[\left(Eh_{sp} \right)^2 + \left(Sh_{nb} \right)^2 \right]^{1/2}$ $h_{sp} = 0.023 \left(\frac{k_l}{D_h} \right) \mathrm{Re}_{lo}^{\ 0.8} \, \mathrm{Pr}_l^{0.4}$ $E = \left[1 + x \, \mathrm{Pr}_l \left(\frac{\rho_l}{\rho_v} - 1 \right) \right]^{0.35}$ $h_{nb} = 55 \, p_{red}^{\ 0.12} \left(-\log_{10} \left(p_{red} \right) \right)^{-0.55} M_w^{\ -0.5} q_{eff}^{\ 0.67}$ $S = \left(1 + 0.55 E^{0.1} \, \mathrm{Re}_{lo}^{\ 0.16} \right)^{-1}$ $Fr_l = \frac{G^2}{g D_h \rho_l}$	(A1)
Steiner and Taborek 1992, [11]	$h_{tp} = \left[\left(Eh_{sp} \right)^3 + \left(Sh_{nb} \right)^3 \right]^{1/3}$ $h_{sp} = 0.023 \left(\frac{k_l}{D_h} \right) \mathrm{Re}_{lo}^{\ 0.8} \, \mathrm{Pr}_l^{0.4}$	(A2)
Warrier et al. 2002, [12]	$h_{tp} = Eh_{sp}$ $h_{sp} = 0.023 \left(\frac{k_l}{D_h} \right) \mathrm{Re}_{lo}^{\ 0.8} \, \mathrm{Pr}_l^{0.4}$ $E = 1 + 6 Bo^{1/16} + f\left(Bo \right) x^{0.65}$ $f\left(Bo \right) = -5.3 \left(1 - 855 Bo \right)$	(A3)